Carburization depth evaluation from magnetic nondestructive testing

Benjamin Ducharne, Yves Armand Tene Deffo, Shurui Zhang, Gael Sebald, Mickaël Lallart, Tetsuya Uchimoto, Christophe Gallais, Olivier Ghibaudo

Carburization depth evaluation from magnetic nondestructive testing

Benjamin Ducharne[1], Yves Armand Tene Deffo[2,3], Shurui Zhang[1,2], Gael Sebald[1], Mickaël Lallart[2], Tetsuya Uchimoto[4], Christophe Gallais[5], Olivier Ghibaudo[5].

[1] ELyTMaX IRL3757, CNRS, Univ Lyon, INSA Lyon, Centrale Lyon, Université Claude Bernard Lyon 1, Tohoku University, Sendai, Japan.

[2] Univ. Lyon, INSA Lyon, LGEF EA682, F-69621, Villeurbanne, France.

[3] Faculty of Engineering and Technology, University of Buea, Buea P.O. Box 63, Cameroon.

[4] Tohoku University, Institute of Fluid Science IFS, Sendai 980-8577, Japan.

[5] Audit et R&T Industriels, SAFRAN TRANSMISSION SYSTEMS, Colombes, France.

Abstract:

Precise estimation of carburization depth is mandatory to avoid failure and critical degradation of high-performance mechanical parts. In this work, we studied magnetic methods as an indirect way to obtain this information. Usual techniques consisting of complex combinations of unrelated indicators have been left aside and replaced by a theoretical approach based on the magnetization mechanisms.

A series of rod specimens were pre-characterized using destructive hardness tests and classified into four categories from virgin to very deep carburization depth. Then, rods from each batch were tested with different magnetic testing techniques. Identical experimental conditions were kept to limit the degrees of freedom and ensure the viability of the conclusions. The Magnetic Incremental Permeability (MIP) maximal amplitude ΔZ which is associated with the domain wall bulging mechanism showed the highest linear correlation with the carburization depth.

Based on these first observations, new experimental conditions were proposed: MIP AC component frequency was reduced to 1 kHz, leading to a magnetic penetration large enough to reach the specimen core. A sudden change in slope was observed on the MIP signature of the treated specimens when the excitation field was close to the core coercivity (of similar magnetic behavior as untreated specimens). The corresponding local slope obtained a very high 0.987 linear correlation coefficient vs. carburization depth and revealed low-frequency MIP as an effective magnetic nondestructive technique for thick carburization evaluation.

Keywords: Metallurgical surface treatments, magnetic incremental permeability, magnetization mechanisms

1 – Introduction

Carburizing, also known as carburization, is a metallurgical treatment in which iron or steel parts absorb carbon while heated in the presence of a carbon-bearing material, like charcoal or carbon monoxide. The purpose of carburization is to make the surface harder. It increases strength and wear resistance. This technique is highly beneficial in preventing corrosion by producing a hard layer (called “case”) on the part surface. Case-depth can range from as low as 200 µm to as deep as 5 mm. Surface hardness can be as high as 800 – 900 HV on the Vickers scale. Case-depth is a fundamental parameter in various applications such as gears, bearings, camshafts, and every mechanical part leading to withstand a sustained applied load [1]-[3].

The two most common heat treatments for surface hardening functional components are carburizing and nitriding. In nitriding, nitrogen atoms replace carbon to diffuse into the surface of the processed parts [4]. In carburizing, the case depth and the carbon content depend on the processing time and the temperature. Longer carburizing times and higher temperatures typically increase the depth of carbon diffusion [5].

For quality inspection, case depth has to be monitored precisely at the end of the manufacturing process. Case depth measurement is sensitive to the type of case hardening, original steel composition, quenching condition, and even the testing method. Most industrial case depth evaluation tests are done destructively. It is measured normal to the finished part surface. The technique consists of sectioning the piece, polishing the surface, and measuring the hardness at regular depth intervals until it drops to the specified range. The effective case depth is then estimated from a location where the hardness number reached a threshold value (around

540 HV for conventional steel) [6]. This method is efficient but meticulous and time-consuming; it also needs to remove and destroy functional parts picked up from production.

Nondestructive methods exist as well. A popular one is the ultrasonic guided wave method, based on the attenuation of Lamb wave, which is proportional to the hardness [7]. This technique gives precise estimation but to be applied, ultrasonic guided wave needs to travel a certain distance, limiting the method to thicker case-depth evaluation. Isotropic radiation, thermal technique, Eddy current testing, and direct-current potential drop measurements are other nondestructive methods giving correlation with hardness and are discussed in the scientific literature [8]-[10]. Still, they are rarely used in the industrial context. The main reason is the prohibitive quantity of data needed by the multi-variant regression analysis used to indirectly evaluate the case depth from the experimental observations [9].

Magnetic methods are other nondestructive popular techniques [11]-[13], and techniques like Magnetic Adaptive Testing have already been proven accurate for the characterization of decarburized specimens [14][15]. Industrial devices based on magnetic signatures have already been commercialized [16]:

- The Stresstech® controller relies on the Magnetic Barkhausen Noise (MBN) analysis [17]. Once correctly set and when carburization remains superficial, this system can provide reasonable case-depth evaluations. Still, a significant problem for this device comes from the quasi-impossibility of distinguishing the effect of hardening treatment from other influent factors (internal stress, dislocations, grain size, texture, plastic strain, precipitates, phase changes, impurities, etc.). This statement is even more critical considering that carburizing acts on these factors.

- The micromagnetic, multi-parametric, microstructure, and stress analysis (3MA®) developed by IZFP Fraunhofer institute is an attractive alternative [18]-[20]. 3MA accumulates and combines data from different magnetization signatures and identifies the ultimate magnetic combination of indicators for case-depth evaluation. 3MA is pragmatic and efficient but needs time-consuming experimental campaigns, leading to non-transposable results. As denoted by Withers et al. [21], NDT magnetic controllers are "mature, but a unified theory relating magnetic signals to basic magnetic parameters is lacking. At present signals are equipment supplier-specific".

In this study, we focused on thick case-depth evaluation (> 500 µm). We opted for the usual magnetic signatures and modified them for improved performance. In industrial equipment, the magnetization mechanisms are triggered simultaneously, and their responses overlap, leading to complex interpretations. Also, working conditions are set to meet the needs of production lines (i.e., high-speed magnetization, etc.), limiting the controlling device capabilities.

Carburization induces profound changes in the magnetic response. Significant gradients are predicted in the boundary separating the case and the core. An ideal way to evaluate case-depth from magnetic measurement is to develop an experimental situation where the most responsive magnetization mechanism can be isolated and easily monitored.

For this, we built an experimental setup and tested different magnetic signatures while keeping the same experimental conditions (sensor, magnetization yoke, etc.) and tried to limit the degrees of freedom. Rod-shaped specimens were tested. The impact of carburization on three distinct magnetic signatures (Magnetic Incremental Permeability (MIP)[22][23], Magnetic

Barkhausen Noise (MBN)[13][24], and classic $B_a(H_{surf})$ hysteresis loops, where B_a is the average cross-section flux density and H_{surf} is the surface tangent excitation field) was checked.

Then, specific indicators were defined as representatives of the different magnetization mechanisms. Pearson coefficients were calculated to verify the linear dependence between the indicators and the case-depth thickness (measured destructively in a preliminary step from a hardness controller on drop samples extracted from the tested specimen batch).

From the associated analysis, conclusions about the most appropriate indicator and magnetization mechanism were drawn. Based on these first observations, we proposed new experimental conditions: MIP alternative contribution frequency was reduced to 1 kHz, leading to a controlled thickness large enough to reach the specimen core. A sudden change in slope was observed in the MIP signature. Then, this local slope was considered a new indicator and led to an outstanding linear coefficient.

This manuscript is organized as follows:

_ The tested specimens are described in the second section. This detailed description includes the hardness measurements and case-depth destructive evaluation performed before the magnetic tests.

_ The magnetic characterization setup is presented in the third section, and the experimental results are provided in the last sub-section.

_ Then, correlations are shown.

_ Improved experimental conditions are proposed, such as an alternative indicator. Together with discussions and conclusions, they constitute the last section of this manuscript.

2 – Tested specimens

A series of rod specimens have been studied in this work (Fig. 1). All specimens were made of 16NiCrMo13 martensitic stainless steel [25]. The chemical composition and the physical properties of 16NiCrMo13 picked up from the literature are provided in Table 1.

- 16NiCrMo13 chemical composition (mass fraction wt.%):

Element	Si	S	P	Ni	Mo	Mn	Cu	Cr	C	Al
min	0.15	-	-	3	0.2	0.3	-	0.8	0.13	-
max	0.40	0.02	0.025	3.5	0.3	0.6	0.35	1.1	0.17	0.05

- 16NiCrMo13 physical properties:

	unit	Typical value
Poisson's coefficient	-	0.3
Heat Capacity	$J \cdot Kg^{-1} \cdot °C^{-1}$	484
Thermal conductivity	$W \cdot m^{-1} \cdot °C^{-1}$	62
Density	-	7.87
Electrical resistivity	μΩ·cm	10
Expansion coefficient	C^{-1}	$11.5\ 10^{6}$
Young modulus	Gpa	200
Yield $R_{p0.2}$	Mpa	1000
Tensile R_m	MPa	1300
Elongation	%	13

Tab. 1 – 16NiCrMo13 chemical composition, mechanical and physical properties.

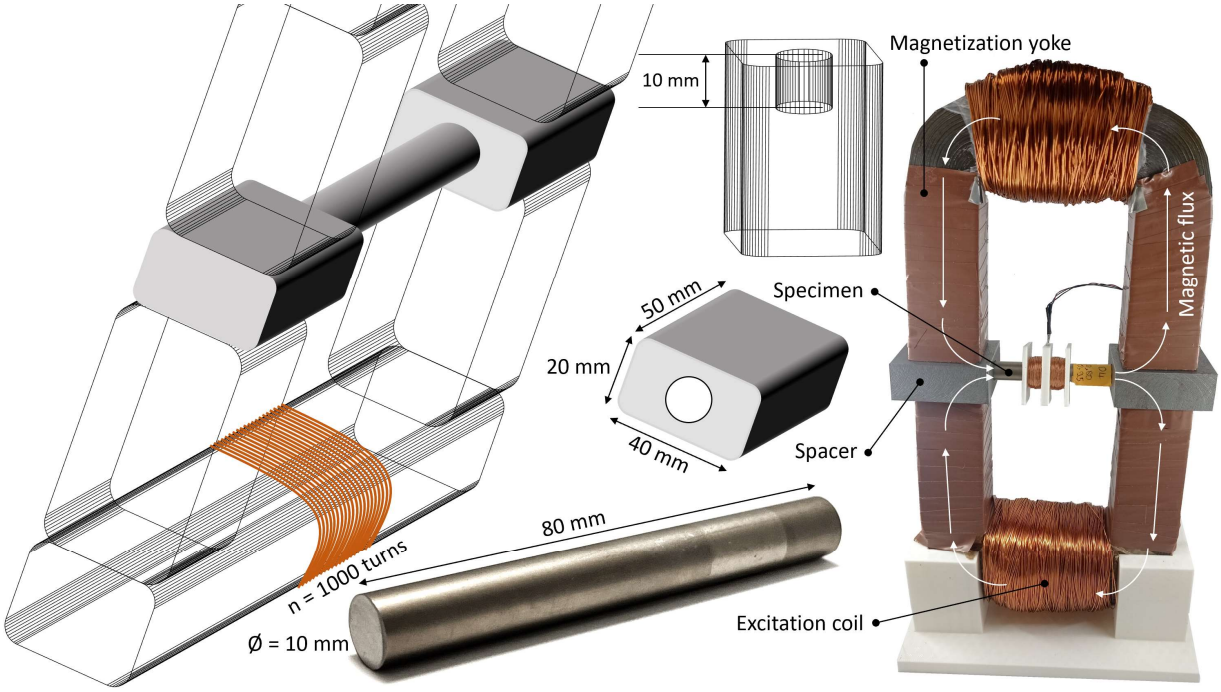

Fig. 1 – Dimensions of the rod-shaped specimens and magnetic testing support illustration.

The series of specimens has been divided into four groups. The first group, called the “control group,” was kept untreated; the other groups were submitted to incremental carburization processes leading to the surface hardness levels displayed in Table 2 and measured from 1 kg load Vickers hardness tests. The hardness threshold defining the case-depth was set to 580 HV.

Sample number	case-depth rod (mm)	
1	-	**control group**
2	-	
3	0.632	**medium treatment**
4	0.683	
5	0.629	
6	0.643	
7	0.877	**Deep treatment**
8	0.861	
9	1.149	**Very deep treatment**
10	1.105	
11	1.142	

Tab. 2 – Case-depth estimation by destructive Vickers hardness characterization.

3 – Magnetic test

3.1 – Ferromagnetism and magnetization mechanisms

Ferromagnetism comes from atomic magnetic moments of electronic origin ordered into small regions called magnetic domains. A magnetic domain includes up to 10^{18} magnetic moments aligned in the same direction and orientation. The domain boundaries called “domain walls” correspond to a progressive change of the atomic magnetic moment direction taking place over hundreds of atoms (depending on energetic equilibrium) [26].

Magnetization in ferromagnetic materials involves complex mechanisms: firstly, the magnetic domains with a magnetization oriented favorably to the applied magnetic field grow, while the unfavorably oriented domains decline in proportion (Fig. 2 – a -> b). Then, the magnetization of the resulting domain, initially oriented along an easy axis, coherently rotates towards the direction of the applied magnetic field (Fig. 2 – c -> d).

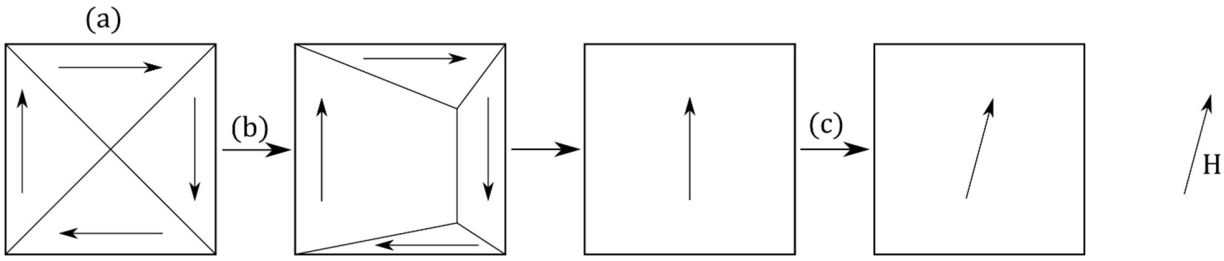

Fig. 2 – Schematic illustration of the magnetization process. (a) Demagnetized state (b) Domain wall motion (c) Magnetization rotation. In practice, the two mechanisms can coincide.

Most of the magnetization mechanisms are associated with the magnetic domains, and more particularly with their kinetic and distribution:

- Domain Wall Bulging (DWB, low H_{surf} amplitude range [27][28]). DWB is associated with local distortions of the domain walls under a low amplitude excitation.
- The Domain Wall's Irreversible Motions (DWIM, middle H_{surf} amplitude range [29][30]). DWIM is associated with the domain wall breaking away from a pinning site under the influence of a medium amplitude excitation.
- The Domains' Nucleation and Fusion (DNF, high H_{surf} amplitude range). FDN happens under high amplitude excitation and includes all domains merging and creation activities.
- The Domain Wall Dynamic Answer (DWDA, frequency dependence, ripples, and avalanches). DWDA is probably more a property than a proper mechanism. It corresponds to the excess energy required by a dynamic magnetization process [28][31]-[33].

The last mechanisms are independent of the magnetic domain structure. These mechanisms include:

- The Magnetization Rotation (MR, high H_{surf} amplitude range)[34]. MR is associated with the rotation of the magnetic moments under the influence of very high excitation.

- The Macroscopic Eddy Currents (MEC, AC H_{surf})[35] constitute the fundament of the Eddy Current Testing (ECT) method.

The magnetic signatures resulting from the practical situations described below give access to a list of specific indicators. Some of them can be considered as privileged images of the magnetization mechanism. Our primary assumption is that carburization will affect each mechanism differently. Therefore, focusing on the most correlated indicator is the solution promoted in this work.

3.2 – Experimental characterization setup

3.2.1 - Magnetic excitation

The magnetic inductor was made of two U-shaped FeSi 3 wt.% yokes. The leg size of the yokes was 37 mm × 37 mm, and the inner distance between the legs was 69 mm. Two steel spacers ensured the magnetic contact between the yokes and the rod specimens (see Fig. 1 for illustration). Both spacers and tested specimens' surface states were visually good, and a limited influence of the mechanical contacts was verified experimentally. The excitation coil was wound around the yokes and supplied by a power amplifier (HSA 4014, NF Corporation, Yokohama, Japan) driven by a frequency generator (Agilent 33220A, Santa Clara, Ca, USA).

3.2.2 - Magnetic instrumentation

a) $B_a(H_{surf})$ major hysteresis cycles

For all magnetic tests, the tangent magnetic field H_{surf} was measured locally on the surface of the tested specimens in the field direction using a hall element sensor (SS94A, Honeywell,

Charlotte, NC, USA). The magnetic response of the Hall element was pre-characterized using a Helmholtz coil driven by a current source in a DC mode.

All the tested specimens were wound with two n = 150 turns sensor coils plugged in series, as illustrated in Fig. 3. These sensors were used for all magnetic tests (MIP alternative component, MBN raw signal, etc.). For $B_a(H_{surf})$ characterization, the voltage drop due to the magnetization variations was recorded using a sirius® acquisition card (Dewesoft, Trbovlje, Slovenia). B_a was obtained by numerical integration (Eq. 3, where S is the cross-section, and e is the electromotive force). A numerical correction was done to cancel the undesired drift due to the ambient noise and the integration process.

$$B_a(t) = -\frac{1}{2n \cdot S}\int_0^t e(t)dt \quad (1)$$

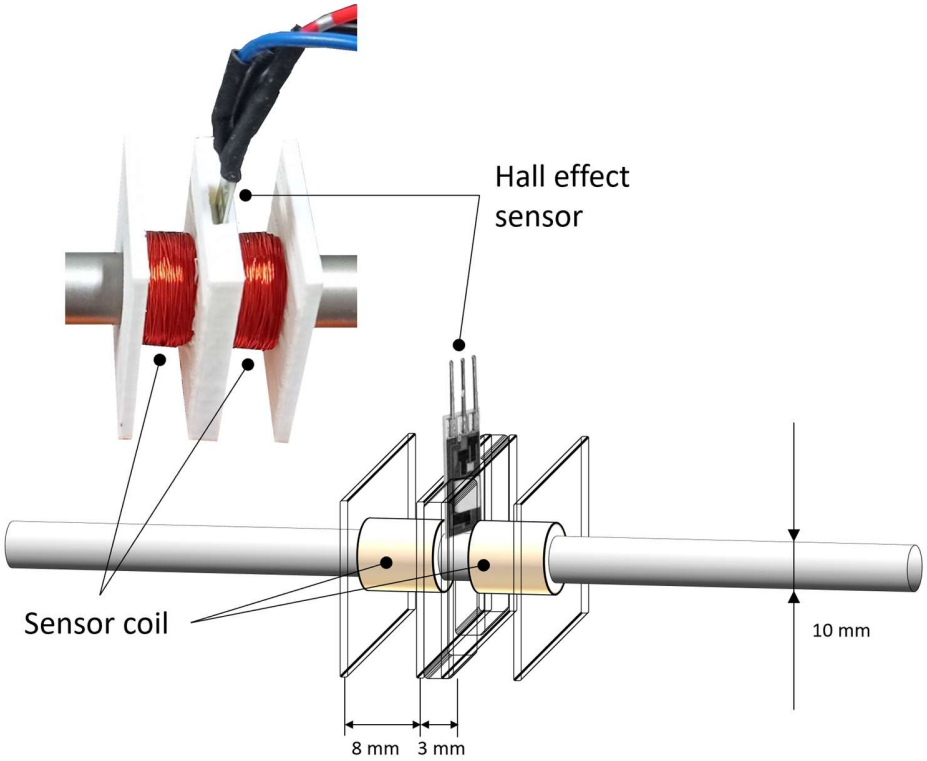

Fig. 3 – Local instrumentation for the magnetic characterization.

b) $Z_{MIP}(H_{surf})$, MIP butterfly cycles

The reversible permeability, observed by superimposing a high-level, quasi-static magnetic field to a high frequency, small amplitude alternating magnetic field, is known as the magnetic incremental permeability [36]. MIP mathematically expression is:

$$\mu_{\mathrm{MIP}} = \frac{1}{\mu_0} \cdot \frac{\Delta \mathrm{B_a}}{\Delta \mathrm{H_{surf}}} \tag{2}$$

where μ_0 is the vacuum permeability, ΔH_{surf} a small variation of H_{surf}, and ΔB_a the related variation of B_a.

The MIP characterization measured the in-series sensor coil impedance using an LCR meter (ZM2375, NF Corporation, Yokohama, Japan). The electrical current in the sensor coil was set to I_{RMS} = 10 mA, inducing a magnetic excitation lower than a quarter of the coercivity (as recommended in the literature [37]). The frequency of the alternative contribution was set to 50 kHz for the first tests and adjusted in the last part of the study. The resulting data provided by the LCR meter consisted of the sensor coil impedance modulus, phase, real and imaginary parts.

b) $MBN_{energy}(H_{surf})$ hysteresis cycles

During the magnetization process, the domain wall motions are stochastic. The MBN raw signal is unpredictable and not reproducible. Time average indicators (RMS, raw signal envelope, etc.) are preferred for the MBN analysis to solve this issue. In this study, we opted for the MBN_{energy} [36][38]:

$$\mathrm{MBN_{energy}(t)} = \int_0^{\mathrm{t}} \mathrm{sign}\left[\frac{\mathrm{dH_{surf}}}{\mathrm{dt}}(\mathrm{s})\right] \mathrm{V_{MBN}^2(s)\,ds} \tag{3}$$

Where V_{MBN} is the sensor coil electromotive force after filtering and amplification. The construction of the MBN_{energy} hysteresis loop from the raw MBN measurement is illustrated in Fig. 4.

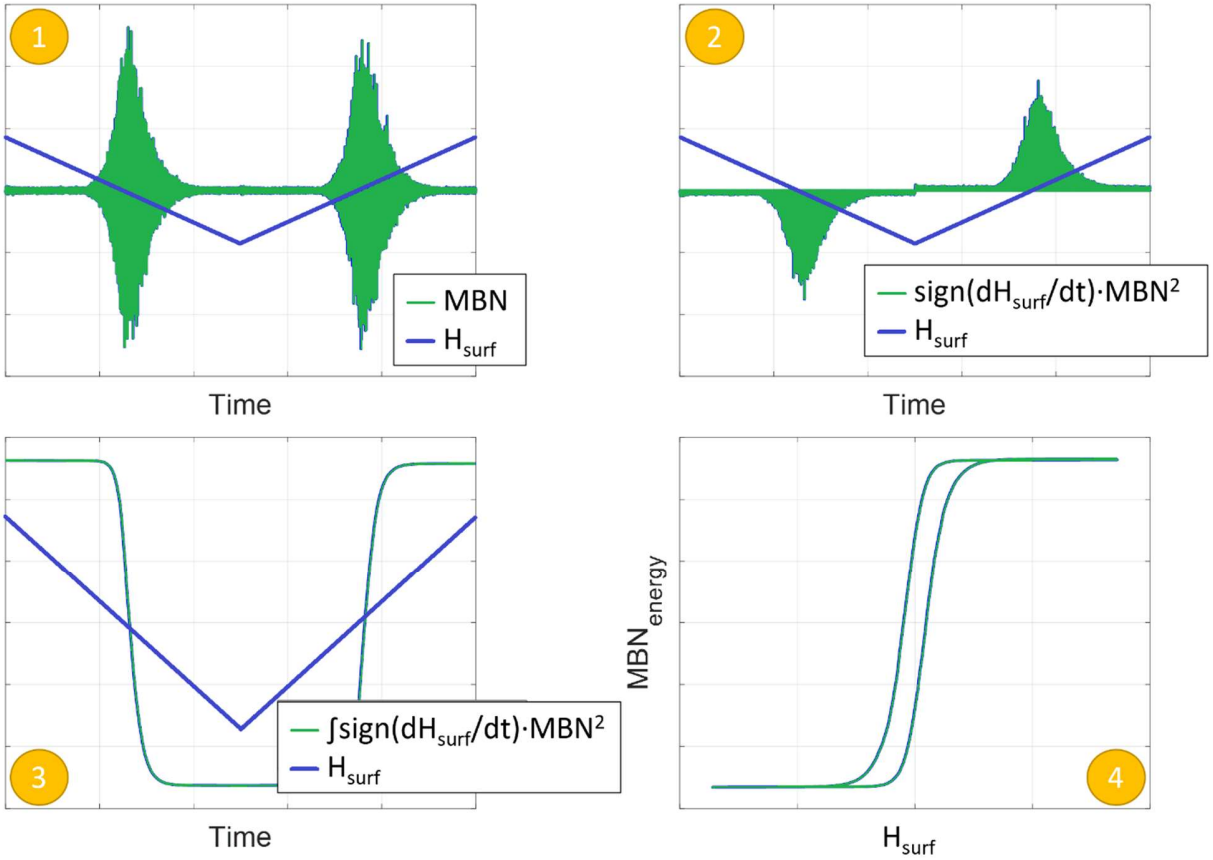

Fig. 4 – $MBN_{energy}(H_{surf})$ hysteresis loop, construction process.

The MBN_{energy} is not *per se* energy, but as explained in [34][38], it can be assimilated as an image of the domain walls' kinetic energy. To compare the $MBN_{energy}(H_{surf})$ and the standard $B_a(H_{surf})$ hysteresis loops, it is possible to renormalize the MBN_{energy} measurement. Two options can be followed for this renormalization:

- equalizing the hysteresis areas, assuming the domain walls motions as fully responsible for the hysteresis loss contribution,

- equalizing the beginning of the saturation elbow (where the rotation mechanism is supposed to start) and considering rotation as a secondary source of hysteresis loss.

In practice, during the experiment, the MBN_{energy} quantity is returned by combining analogic and numerical procedures:

- The sensor coil raw electromotive force is filtered and amplified using a Stanford Research SR650 (Sunnyvale, CA, USA). The cut-off frequencies were set to 1 and 30 kHz, and the gain to 90 dB·dec^{-1}.
- The square (Step 2, Fig. 4), the integration (Step 3, Fig. 4), and a drift correction were done numerically using Matlab® software.

All the data were averaged over four excitation periods to reduce the parasitic noises.

3.2.3 – Experimental results

a) Raw results

The first results depicted in Fig. 5 show the magnetic signatures described in sub-section 3.2.2 and measured for all specimens.

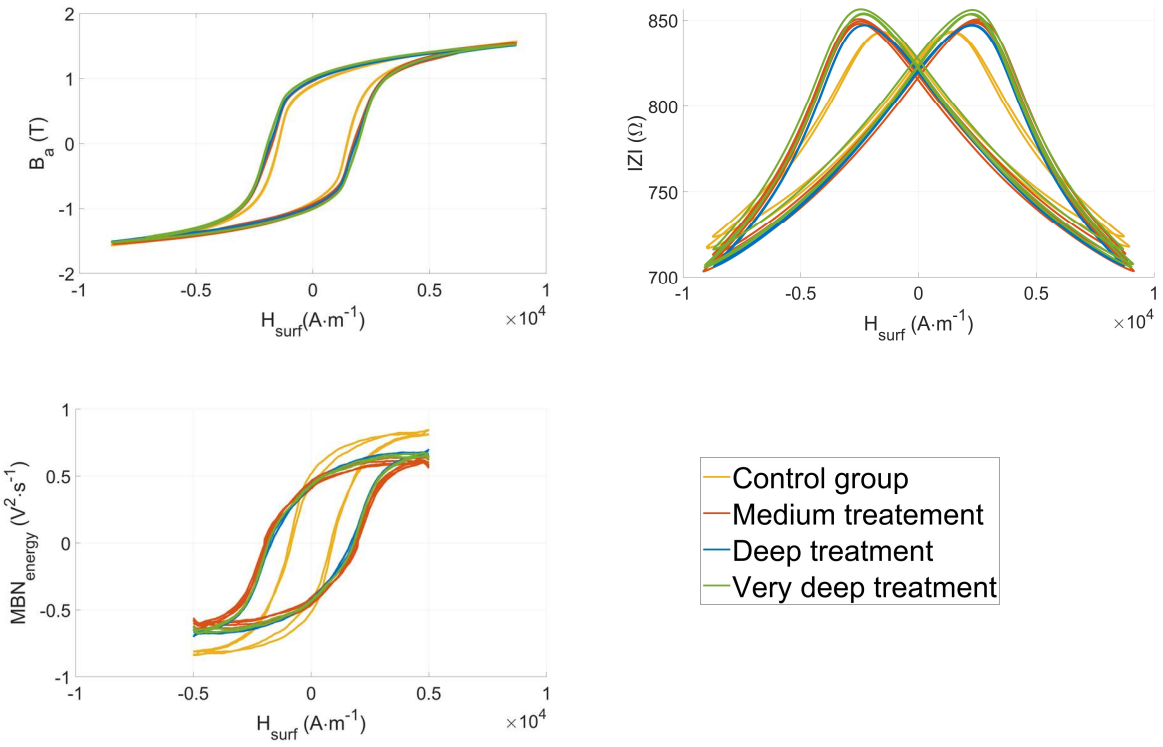

Fig. 5 – $B_a(H_{surf})$, $IZI(H_{surf})$, and $MBN_{energy}(H_{surf})$ for all tested specimens.

Once saturated, the $MBN_{energy}(H_{surf})$ hysteresis cycles get noisy. Thus, for those cycles, $max(H_{surf})$ was limited to 5000 $A{\cdot}m^{-1}$.

The significant differences between the treated and the virgin specimens observed for all magnetic signatures are worth noting.

b) Magnetic indicators vs. magnetization mechanisms and correlations

A list of magnetic indicators read on Fig. 5 signatures and selected for their privileged relationship with the magnetization mechanisms was established:

_ MIP alternative contribution amplitude is set low enough to avoid DWIM (Domain Wall's Irreversible Motions) but allowed DWB (Domain Wall Bulging). Thus, $\Delta Z = max(Z) - min(Z)$ constitutes a good DWB image.

_ Coercivities read on MIP, MBN, and $B_a(H_{surf})$ are close and mainly due to DWIM. Still, we opted for MBN coercivity as a DWIM representative. Even low, other mechanisms might influence the coercivity of the other signatures (like MR for $B_a(H_{surf})$).

_ MBN_{energy} is an image of the domain wall velocity and DWDA (Domain Wall Dynamic Answer).

_ MR is preponderant once the $B_a(H_{surf})$ cycle is closing (in the very high saturation level). Then, μ_{sat} the saturation permeability has been selected as MR representant.

_ Remanence read on the $IZI(H_{surf})$ MIP cycle was chosen as MEC representative. Remanence is obtained when the quasi-static contribution is null, and the MIP answer solely depends on MEC associated with the high-frequency behavior.

Table 3 shows these indicators and their associated magnetization mechanisms:

magnetization mechanism	magnetic indicator
Domain Wall Bulging - DWB	ΔZ - (MIP)
Domain Wall's Irreversible Motions - DWIM	Coercivity - (MBN)
Domains' Nucleation and Fusion - DNF	-
Domain Wall Dynamic Answer - DWDA	$\max(MBN_{energy})$ - (MBN)
Magnetization Rotation - MR	μ_{sat} - $(B_a(H_{surf}))$
Macroscopic Eddy Currents - MEC	Remanence - (MIP)

Tab. 3 – Magnetization mechanisms and their associated magnetic indicators.

The absence of DNF indicator is worth noting. DNF is not associated with a feasible observation from human-scale magnetic characterization equipment, and the energy exchanges related to this mechanism are weak.

In the next step, Pearson coefficients were calculated to verify the linear correlation between the case-depth measurements (Table 2) and the magnetization mechanisms represented by their

specific indicators. Fig. 6 illustrates these correlations by depicting the evolution of the magnetic indicators vs. case-depth.

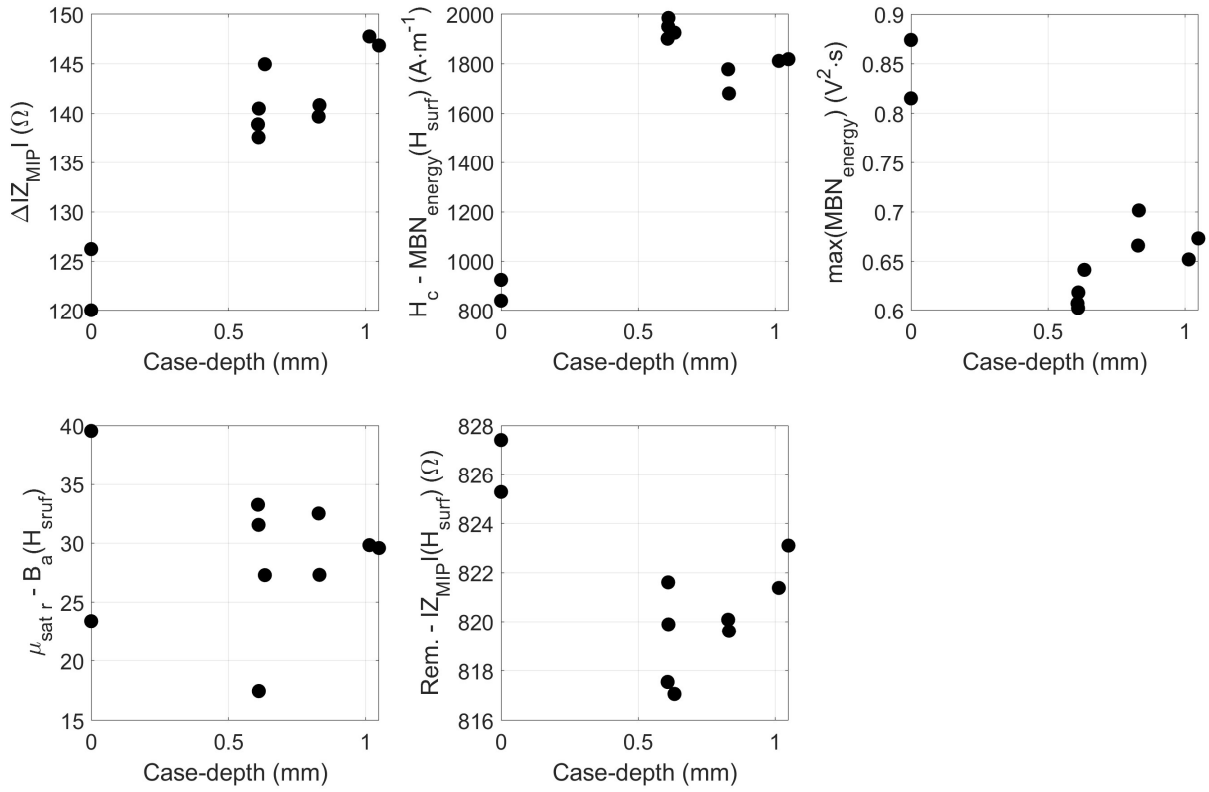

Fig. 6 – Magnetic indicators evolution as a function of case-depth.

With almost 0.94, DWB showed the highest Pearson coefficient. Multiple reasons can be given for this, including the evolution of the microstructural properties during the carbon diffusion process. By giving rise to more or stronger hinder defects, the magnetic domains' kinetic is profoundly modified, affecting DWB and indirectly ΔZ read on the MIP curve. This observation could also explain the good results of DWIM and the overall historical focus on MBN as a case-depth magnetic characterization method.

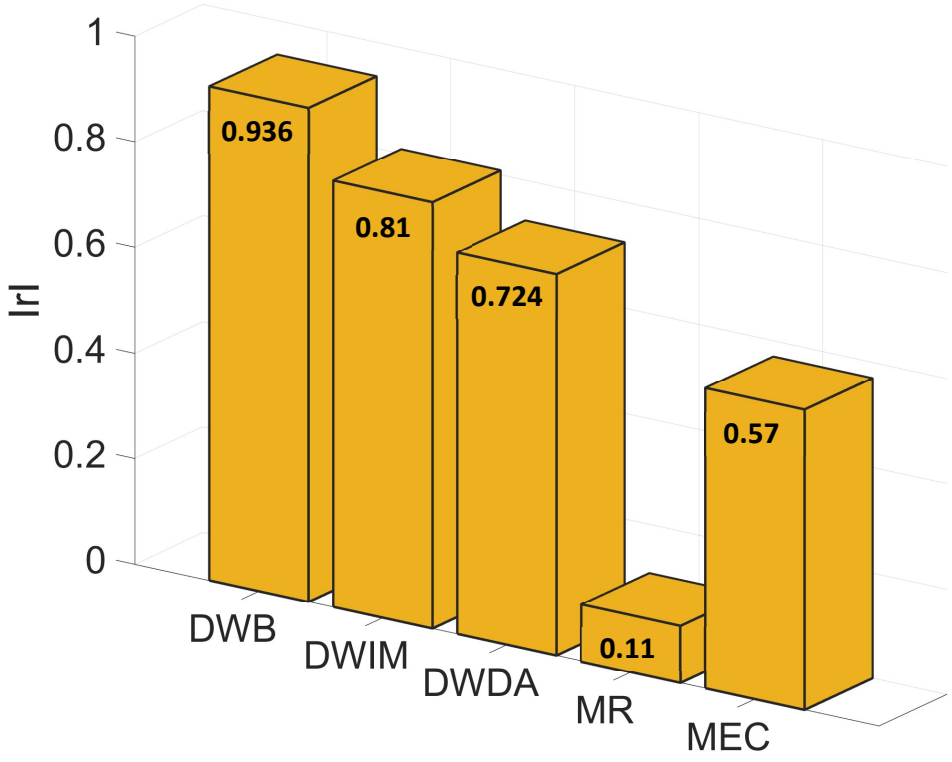

Fig. 7 – Pearson linear correlation coefficients, magnetic indicators vs. case-depth.

4 – Low-frequency MIP, an ideal way to magnetically characterize thick case-depth

Section 3 conclusions highlight the use of DWB and MIP as the most case-depth correlated magnetization mechanism and the best magnetic signature. Still, the way MIP has been tested with a 50 kHz alternative contribution (accordingly to the literature recommendation [37][39]), limits the thickness of a scanned area to the tested specimen's upper layers due to

electromagnetic skin effect (δ ≈ 100 µm for permeabilities in the range of the MIP measured ones).

Additional MIP tests were tried in the low-frequency range to overcome this issue and find even better indicators. Different frequencies have been tested, but the best results displayed in Fig. 8 were obtained at 1kHz.

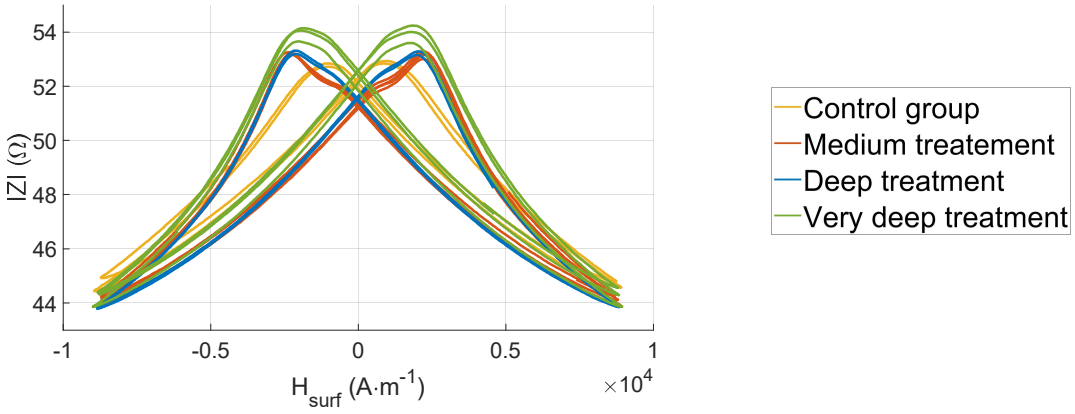

Fig. 8 – 1 kHz, IZI(H_{surf}) MIP curves for all tested specimens.

Interestingly, a sudden local change in slope is visible on the treated specimens, and this observation is even more evident in the angle(Z)(H_{surf}) curves depicted in the chart below (Fig. 9)

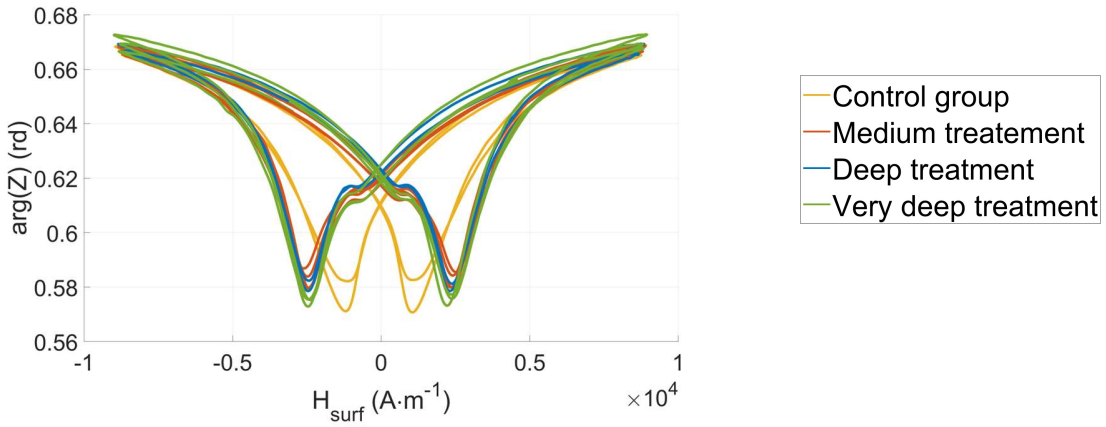

Fig. 9 – 1 kHz, angle(Z)(H_{surf}) MIP curves for all tested specimens.

This sudden local change in slope appeared to be highly correlated to the carburization treatment. This can be explained by the distinct magnetic behaviors between the specimens' core (untreated and softer, magnetically speaking) and the carburized upper layer. The carbon diffusion leads to the precipitation of carbides which, from a magnetization point of view, generates hinder points and hardens the magnetic behavior (enlarged coercive field and reduced differential permeability).

By decreasing the MIP alternative frequency range, the scanned thickness becomes large enough to reach the uncarburized specimen core and generate a second peak at a lower excitation level on the $|Z|(H_{surf})$ MIP signature. Of course, just like hardness, the change in the magnetic answer is continuous and takes the form of a gradient; still, the difference between the surface and the core behaviors is strong enough to induce such significant differences in the MIP answer.

Based on this observation, a new indicator was defined: the slope $d|Z|/dH_{surf}$ at $H_{surf} = H_{c\ virgin\ sample}$ (where $H_{c\ virgin\ sample}$ is the coercivity of the virgin specimen, i.e., untreated by carburization). $H_{c\ virgin\ sample}$ is easy to find from our characterization and corresponds to the value of H_{surf} when $|Z|$ is maximal on the MIP curve of the virgin specimens.

Fig. 10 gives an illustration of this new indicator.

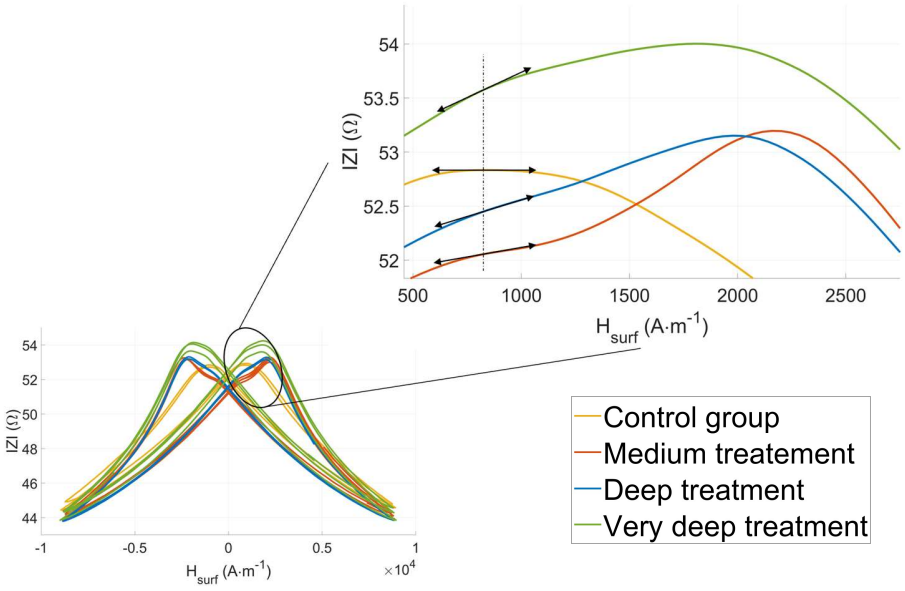

Fig. 10 – $dIZI/dH_{surf}$ at $H_{surf} = H_{c\ virgin\ sample}$ indicator illustration.

Once $dIZI/dH_{surf}$ at $H_{surf} = H_{c\ virgin\ sample}$ was determined for all specimens, it was plotted as a function of case-depth (Fig. 11), and the linear correlation coefficient was calculated.

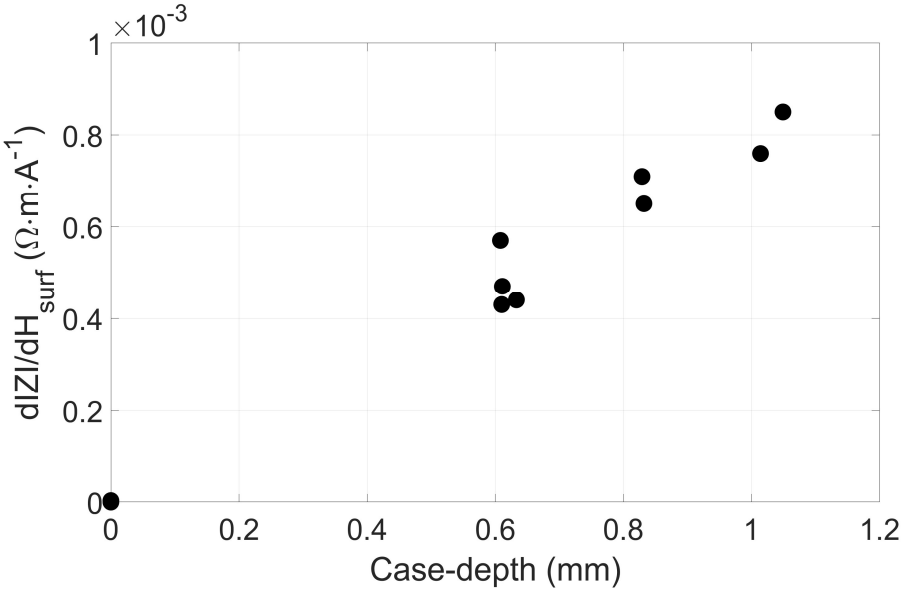

Fig. 11 – $dIZI/dH_{surf}$ at $H_{surf} = H_{c\ virgin\ sample}$ vs. case-depth.

Remarkably, this coefficient reached the outstanding value of 0.987 and confirmed our expectations about $dIZI/dH_{surf}$ at $H_{surf} = H_{c\ virgin\ sample}$ being an excellent case-depth indicator.

5 – Conclusion

Carburization is a metallurgical surface treatment performed on high-performance mechanical parts. Making the specimen's upper layer harder increases strength and wear resistance and helps prevent corrosion. For quality certification, it is required that the carburization process and the resulting case-depth to be monitored during the whole manufacturing process.

This study focused on magnetic control to evaluate thick case-depth carburization. A series of rod-shaped specimens treated with different carburization levels and pre-characterized case-depth were tested with different magnetic signatures.

Specific magnetic indicators were selected as privileged representatives of the magnetization mechanisms and tested vs. case-depth. Domain wall bulging associated with ΔZ – (MIP) was the most correlated mechanism.

Based on this first conclusion, a new configuration of incremental permeability was proposed to obtain a scan area thick enough to reach the untreated specimen core. A new indicator still associated with the sensitive domain wall bulging was tested ($dIZI/dH_{surf}$ at $H_{surf} = H_{c\ virgin\ sample}$) and reached the very high 0.987 linear correlation vs. case-depth.

This study highlighted low-frequency magnetic incremental permeability as a powerful magnetic signature for thick case-depth characterization. Of course, the number of tests was limited. These first exciting results must be confirmed, including on specimens of different

natures. Geometry also has a critical influence on the magnetic answer. Even if not described in this manuscript, recent tests on flat plate specimens with a small-diameter pancake coil have led to similar correlations, allowing us to conclude with the universality of the observations.

It is worth reminding here of the MIP simplicity, which can be implemented efficiently on the production lines and generates no pollution. Good results were obtained at 1 kHz, but a frequency sweep for the AC contribution could lead to alternative indicators giving access to an even more accurate description of the carburization levels.

Besides carburization, other metallurgical treatments can potentially generate thick layer modifications (shot peening, etc.). From the perspective of this work, it would be interesting to test our method and the selected indicators in such new configurations.

Finally, simulation tools have been developed for years to simulate the magnetic answer and the overall electromagnetic conversion of such NDT situations (wound coil, etc.). By combining simulation results and new indicators, significant progress should be forecasted in understanding the carburization process and its consequences on the magnetization answer. For this, models considering a gradient of the physical properties would be the most valuable.

References

[1] Parrish, G., 1999. *Carburizing: microstructures and properties*. Asm International.

[2] Edenhofer, B., Joritz, D., Rink, M. and Voges, K., 2015. Carburizing of steels. In *Thermochemical Surface Engineering of Steels* (pp. 485-553). Woodhead Publishing.

[3] Rahmel, A., Grabke, H.J. and Steinkusch, W., 1998. Carburization–introductory survey. *Materials and corrosion*, *49*(4), pp.221-225.

[4] Steiner, T. and Mittemeijer, E.J., 2016. Alloying element nitride development in ferritic Fe-based materials upon nitriding: A review. *Journal of materials engineering and performance*, *25*(6), pp.2091-2102.

[5] Boyle, E., Northwood, D.O., Bowers, R., Sun, X. and Bauerle, P., 2009. Microstructural effects on residual stress, retained austenite, and case depth of carburized automotive steels. *SAE International Journal of Materials and Manufacturing*, *1*(1), pp.697-708.

[6] Mittemeijer, E.J., 2013. Steel Heat treating Fundamentals and Processes. *ASM Handbook A*, *4*, p.2013.

[7] Belanger, P., 2010. *Feasibility of thickness mapping using ultrasonic guided waves* (Doctoral dissertation, Department of Mechanical Engineering, Imperial College London).

[8] Chan, S.C., Grimberg, R., Hejase, J.A., Zeng, Z., Lekeakatakunju, P., Udpa, L. and Udpa, S.S., 2010. Nonlinear eddy current technique for characterizing case hardening profiles. *IEEE transactions on magnetics*, *46*(6), pp.1821-1824.

[9] Bowler, J.R., Huang, Y., Sun, H., Brown, J. and Bowler, N., 2008. Alternating current potential-drop measurement of the depth of case hardening in steel rods. *Measurement Science and Technology*, *19*(7), p.075204.

[10] Guo, X., Sivagurunathan, K., Garcia, J., Mandelis, A., Giunta, S. and Milletari, S., 2009. Laser photothermal radiometric instrumentation for fast in-line industrial steel hardness inspection and case depth measurements. *Applied optics*, *48*(7), pp.C11-C23.

[11] Kobayashi, S., Takahashi, H. and Kamada, Y., 2013. Evaluation of case depth in induction-hardened steels: Magnetic hysteresis measurements and hardness-depth profiling by differential permeability analysis. *Journal of magnetism and magnetic materials*, *343*, pp.112-118.

[12] Zhang, C., Bowler, N. and Lo, C., 2009. Magnetic characterization of surface-hardened steel. *Journal of Magnetism and Magnetic Materials*, *321*(23), pp.3878-3887.

[13] Santa-Aho, S., Vippola, M., Sorsa, A., Leiviskä, K., Lindgren, M. and Lepistö, T., 2012. Utilization of Barkhausen noise magnetizing sweeps for case-depth detection from hardened steel. *Ndt & E International*, *52*, pp.95-102.

[14] Perevertov, O., Stupakov, O., Tomáš, I. and Skrbek, B., 2011. Detection of spring steel surface decarburization by magnetic hysteresis measurements. *Ndt & E International*, *44*(6), pp.490-494.

[15] Skrbek, B., Tomáš, I., Kadlecová, J. and Ganev, N., 2011. NDT characterization of decarburization of steel after long-time annealing. *Kovove Mater*, *49*, pp.401-409.

[16] Omar, M. ed., 2012. *Nondestructive Testing Methods and New Applications*. BoD–Books on Demand.

[17] Tam, P.L., Hammersberg, P., Persson, G. and Olavison, J., 2021. Case depth evaluation of induction-hardened camshaft by using magnetic Barkhausen noise (MBN) method. *Nondestructive Testing and Evaluation*, *36*(5), pp.494-514.

[18] Dobmann, G., 2007. Physical basics and industrial applications of 3MA–micromagnetic multiparameter microstructure and stress analysis. *Fraunhofer IZFP, Saarbrcken, Germany*, pp.1-17.

[19] Mironenko, I., Szielasko, K., Kiselmann, I., Koop, H., Koop, M., Altpeter, I., Dobmann, G. and Boller, C., 2011. Wideband micromagnetic multi-parameter materials characterization with 3MA. In *Proceedings of the 9th International Conference on Barkhausen Noise and Micromagnetic Testing*.

[20] Jedamski, R. and Epp, J., 2020. Nondestructive micromagnetic determination of hardness and case hardening depth using linear regression analysis and artificial neural networks. *Metals*, *11*(1), p.18.

[21] Withers, P.J., Turski, M., Edwards, L., Bouchard, P.J. and Buttle, D.J., 2008. Recent advances in residual stress measurement. *International Journal of Pressure Vessels and Piping*, *85*(3), pp.118-127.

[22] Gupta, B., Uchimoto, T., Ducharne, B., Sebald, G., Miyazaki, T. and Takagi, T., 2019. Magnetic incremental permeability nondestructive evaluation of 12 Cr-Mo-WV Steel creep test samples with varied ageing levels and thermal treatments. *NDT & E International*, *104*, pp.42-50.

[23] Yashan, A. and Dobmann, G., 2002. using eddy current coil in the presence of magnetic hysteresis. *Electromagnetic Nondestructive Evaluation (VI)*, *6*, p.150.

[24] Ducharne, B., 2020. Micromagnetic nondestructive testing Barkhausen noise vs other techniques. In *Barkhausen Noise for Nondestructive Testing and Materials Characterization in Low-Carbon Steels* (pp. 223-238). Woodhead Publishing.

[25] El Ghazal, H., 1999. *Etude des propriétés microstructurales et mécaniques des aciers 16NiCrMo13 cémenté et 32CrMoV13 nitrure: application à la prévision de leur limite d'endurance en fatigue de roulement* (Doctoral dissertation, Lyon, INSA).

[26] Cullity, B.D. and Graham, C.D., 2011. *Introduction to magnetic materials*. John Wiley & Sons.

[27] R. Valenzuela, I. Betancourt, “Giant magnetoimpedance, skin depth, and domain wall dynamics,” *IEEE Trans. Mag.*, vol. 38, iss. 5, pp. 3081 – 3083, 2002.

[28] Ducharne, B., Zhang, S., Sebald, G., Takeda, S. and Uchimoto, T., 2022. Electrical steel dynamic behavior quantitated by inductance spectroscopy: Toward prediction of magnetic losses. *Journal of Magnetism and Magnetic Materials*, *560*, p.169672.

[29] F. Qiu, M.J. Klug, G. Tian, P. Hu, J. McCord, “Influence of magnetic domain wall orientation on Barkhausen noise and magneto-mechanical behavior in electrical steel,” *J. Phys. D: App. Phys.*, vol. 52, 265001, 2019.

[30] Jiles, D.C., 2000. Dynamics of domain magnetization and the Barkhausen effect. *Czechoslovak journal of physics*, *50*(8), pp.893-924.

[31] S.E. Zirka, Y.I. Moroz, P. Marketos, A.J. Moses, “Viscosity-based magnetodynamic model of soft magnetic materials,” *IEEE Trans. Mag.*, vol. 42, n°9, pp. 2121 – 2132, 2006.

[32] M.A. Raulet, B. Ducharne, J.P. Masson, and G. Bayada, “The magnetic field diffusion equation including dynamic hysteresis: a linear formulation of the problem,” *IEEE Trans. Mag.,* Vol. 40, n° 2, pp. 872-875, 2004.

[33] M. Petrun, S. Steentjes, “Iron-loss and magnetization dynamics in non-oriented electrical steel: 1-D Excitations up to high frequencies,” *IEEE Access*, vol. 8, pp. 4568-4593, 2020.

[34] Fagan, P., Ducharne, B., Daniel, L. and Skarlatos, A., 2021. Multiscale modelling of the magnetic Barkhausen noise energy cycles. *Journal of Magnetism and Magnetic Materials*, *517*, p.167395.

[35] M. Carara, M. N. Baibich, R. L. Sommer, “Magnetization dynamics as derived from magneto impedance measurements,” *J. App. Phys.*, vol. 88, n°1, pp. 331 – 335, 2000.

[36] B. Gupta, B. Ducharne, T. Uchimoto, G. Sebald, T. Miyazaki, T. Takagi, “Comparison of electromagnetic inspection methods for creep-degraded high chromium ferritic steels,” *NDT&E Int.*, vol. 118, 102399, 2021.

[37] A. Yashan, G. Dobmann, “Measurements and semi-analytical modeling of incremental permeability using eddy current coil in the presence of magnetic hysteresis”, in: F. Kojima, T. Takagi, S.S. Udpa, J. Pávó (Eds.), Electromagnetic Nondestructive Evaluation (VI), IOS press, pp. 150-157, 2002.

[38] Fagan, P., Ducharne, B., Daniel, L., Skarlatos, A., Domenjoud, M. and Reboud, C., 2022. Effect of stress on the magnetic Barkhausen noise energy cycles: A route for stress evaluation in ferromagnetic materials. *Materials Science and Engineering: B*, *278*, p.115650.

[39] Matsumoto, T., Uchimoto, T., Takagi, T., Dobmann, G., Ducharne, B., Oozono, S. and Yuya, H., 2019. Investigation of electromagnetic nondestructive evaluation of residual strain in low carbon steels using the eddy current magnetic signature (EC-MS) method. *Journal of Magnetism and Magnetic Materials*, *479*, pp.212-221.